Journal of Materials Chemistry A

Accepted Manuscript

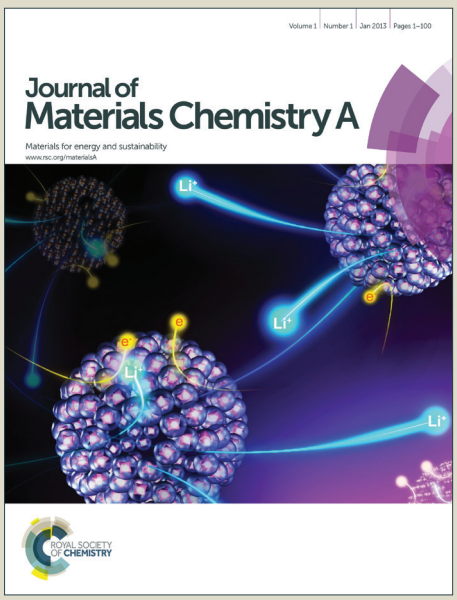

ROYAL SOCIETY OF CHEMISTRY

www.rsc.org/materialsA

Journal of
Materials Chemistry A

COMMUNICATION

View Article Online
View Journal | View Issue

Received (in xxx, xxx) xxth xxxx 20xx,
Accepted xxth xxxxx 20xx

DOI: 10.1039/c0xx00000x

Ce_2O_2S anchored on graphitized carbon with tunable architectures as a new promising anode for Li-ion batteries

Juhong Cheng[a,1], Jinliang Zhu[a,1], Xiaolin Wei[b], Pei Kang Shen[a,*]

Cite this: DOI: 10.1039/c0xx00000x

www.rsc. org/MaterialA

Flower-like and dicranopteris-like Ce_2O_2S/carbon composites have been originally prepared by the heat treatment of S-containing ion-exchange resin and cerium acetate. The structure and morphology of the Ce_2O_2S /carbon are investigated by XRD, SEM, TEM and STEM. The flower-like Ce_2O_2S is self-assembled by porous single crystalline Ce_2O_2S sheets which are well anchored on carbon. The dicranopteris-like Ce_2O_2S/carbon is also comprised by single crystalline 'Ce_2O_2S leaves' surrounded by a carbon layer. Electrochemical performances of flower-like and dicranopteris-like Ce_2O_2S/carbon are studied by CV, galvanostatic discharge-charge tests and electrochemical impedance spectroscopy (EIS) measurements. The results show that the Ce_2O_2S/carbon has stable specific capacity up to 627 mAh/g after 180 cycles at a constant current density of 50 mA/g between 0.01 and 3V. This performance can be a choice as a potential anode material for Li-ion batteries.

1. Introduction

Lithium-ion batteries (LIB), as one of the important power resources for portable electronic devices and electric vehicles, have been attracting much attention in the scientific and industrial fields[1]. As the most common anode material used in Li-ion batteries, graphite has a theoretical capacity of 370 mAh/g. To overcome the limited capacity of the graphite anode, alternatives with higher capacity such as metal oxides and sulfides have been intensively investigated as promising anode materials[2,3]. CeO_2 as one of the metal oxides has been used as LIB anode materials and nano-additive in LIBs[4-6] including pure CeO_2 solid powder[7,8], hollow spheres[9] and CeO_2/carbon composite[10]. Sun's group reported that the substitution of some S for O in $LiMn_2O_4$ (oxysulfide $LiMn_2O_{3.98}S_{0.02}$) improved the cycling performance in LIBs[11]. Abraham and co-workers reported that ternary oxysulfides like MoO_xS_y obviously displayed preferable electrochemical performance compared with binary metal sulfides[12]. Recently, it was also reported that metal oxysulfides, such as $LaGaS_2O$[13] and $Bi_4O_4Se_3$[14] exhibited unique electronic properties compared with metal oxides. However, to the best of our knowledge, the electrochemical performance of Ce_2O_2S in lithium-ion batteries has not been reported.

Herein, we report a facile method to synthesize Ce_2O_2S nanoparticles anchored on graphitized carbon with tunable flower-like and dicranopteris-like architectures through the thermolysis of S-containing ion-exchange resin and cerium acetate. The novel method is developed on the basis of the following three key considerations. Firstly, the uniformly dispersed S-containing resin provides sulfur resource to produce Ce_2O_2S. Secondly, the resin decomposed into graphitized carbon during the pyrolysis and coated on the surface of Ce_2O_2S, which serves as a buffer coating and prevent the reuniting of Ce_2O_2S during the insertion and extraction of lithium ions. Thirdly, the graphitized carbon layer with an excellent conductivity provides a highway for electron transport. The obtained Ce_2O_2S/carbon exhibited excellent cycling stability, rate capability and high reversible lithium storage capacity.

2. Experimental

2.1. Materials synthesis

In a typical synthesis, cerium (III) acetate hydrate (2.5 mmol) was mixed with thiourea resin (1.5 g) in deionized water and diethanolamine, followed by hydrothermal synthesis at 250 °C for 24 h. The produced precursor was collected and purified by filtration the suspension liquid. Then, the dried precursor was heated at 1000 °C in N_2 atmosphere for 1 h. The flower-like Ce_2O_2S/carbon composites were obtained. The dicranopteris-like Ce_2O_2S/carbon composites were obtained by using deionized water and triethylamine as the solvent during the hydrothermal synthesis.

2.2. Physicochemical characterization

The X-Ray powder diffraction (XRD) measurements were performed on a D/Max-III (Rigaku Co., Japan) with Cu Kα radiation source (30 kV and 30 mA), recorded at a scan rate of 10° (2θ) min^{-1}. The morphology characterization was

performed on a scan electron microscopy (SEM) (Quanta 400 FEG, FEI Company). The transmission electron microscopy (TEM) and element mapping investigations were carried out on a JEOL JEM-2010 (JEOL Ltd.) operating at 200 kV and FEI Tecnai G2 F30. The N_2 adsorption experiments using an ASAP 2420 Surface Area Analyzer (Micrometeritics Co., USA) were conducted to investigate the porosity of the samples.

2.3. Electrochemical characterization

The collected Ce_2O_2S/carbon was mixed with acetylene black and polyvinylidene fluoride (PVDF) at a weight ratio of 80:10:10 in N-methyl-2-pyrrolidene (NMP) solution and stirred for 5 h. The obtained slurry was coated on clean copper foil and dried in vacuum oven at 120 °C for 10 h and then was pressed and cut into discs. The 2032 coin-type cells were assembled in an argon-filled glove box using pure lithium as the anode, 1 mol/L $LiPF_6$/EC+DMC+EMC (1:1:1) (Shenzhen Capchem Technology Co., Ltd, China) as the electrolyte and micro-porous membrane (Celguard 2400, USA) as the separator. The cells were galvanostatically charged and discharged between 0.01 V and 3 V versus lithium at room temperature on a program-controlled test system (Shenzhen Neware Battery Co., China). The cyclic voltammetric measurements and electrochemical impedance spectroscopy (EIS) measurements were performed on an IM6e electrochemical workstation (Zahner-Electrik, Germany).

3. Results and discussion

Fig.1a shows the XRD pattern of the Ce_2O_2S/carbon composites and the model structure of the Ce_2O_2S. The main diffraction peaks at 2θ = 25.6°, 28.8°, 36.8°, 45.2°, 47.7° and 52.9° are assigned to (100), (101), (012), (110), (103) and (112) facets of Ce_2O_2S (PDF# 75-1931), respectively. The broad peak around 26° is attributed to carbon in the composites. The carbon may be explained by the carbonization from the resin during the subsequent heat treatment. The fact that no other peaks could be found in the pattern indicates that this synthesis approach can produce highly pure Ce_2O_2S/carbon composites.

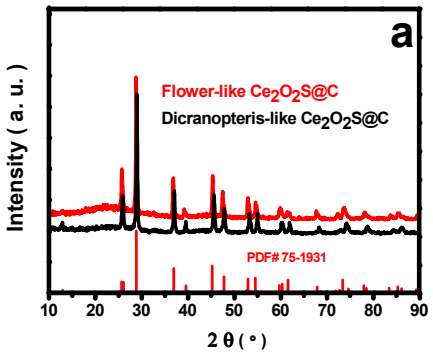

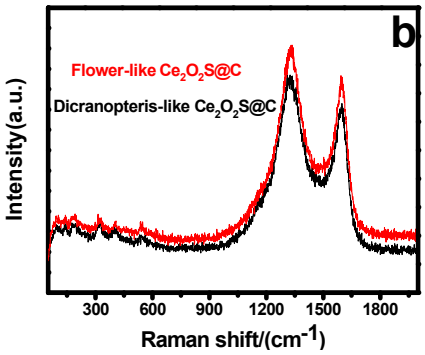

Fig.1 (a) XRD pattern of the Ce_2O_2S /carbon composites and (b) Raman spectrum of the Ce_2O_2S /carbon composite.

The type of carbon species in the composites was investigated by the Raman spectroscopy (Fig. 1b). The band observed at 1340 cm^{-1} is the D-band，which is attributed to the vibrations of carbon atoms with dangling bonds in disordered graphite planes and the defects incorporated into pentagon and heptagon graphite-like structures. The G-band at 1596 cm^{-1} corresponds to a splitting of the E2g stretching mode of graphite and reflects the structural intensity of the sp^2-hybridized carbon atom[15]. The band between 50 and 600 cm^{-1} is attributed to the cerium oxysulfide.

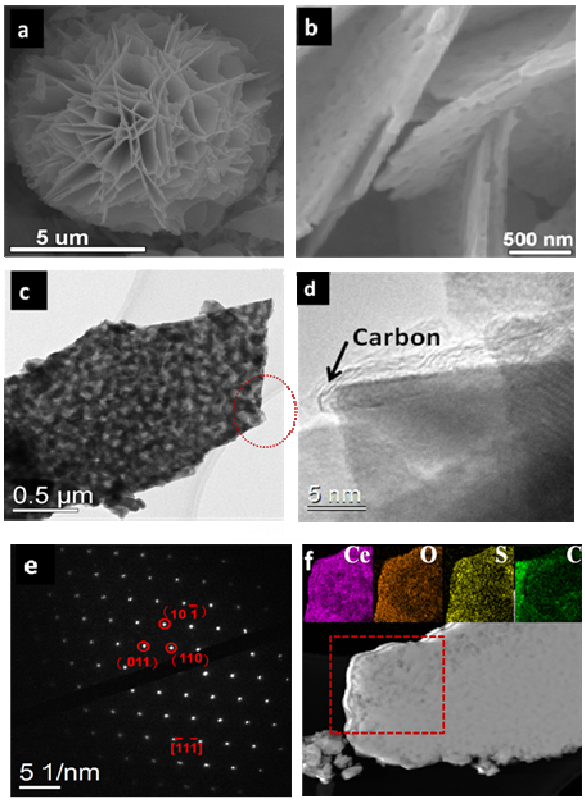

Fig.2 (a,b) SEM images of the flower-like Ce_2O_2S@carbon composites, (c,d) TEM images, (e) SAED pattern of a typical isolated Ce_2O_2S@carbon nanosheet (corresponding to fig.2c)

and (f) STEM-HAADF image and element mapping images of one Ce_2O_2S@carbon nanosheet.

Fig. 2 shows the morphology of samples obtained by using deionized water and diethanolamine. Fig. 2a shows the scanning electron microscope (SEM) image of the representative flower-like Ce_2O_2S/carbon composite with a diameter of 8 μm. The magnified SEM image in Fig. 2b demonstrated that the micro-flower exhibits a hierarchical structure. The flower-like microspheres are assembled by many intercrossed nanosheets with an average thickness of about 60 nm. Interestingly, a large number of pores were clearly observed on each nanosheet, which can increase the active sites and favorable for the diffusion of lithium ions[16-18]. Further insight into the morphology and micro-structure of the flowers was obtained by TEM. Fig. 2c presents a TEM image for a typical isolated Ce_2O_2S@carbon nanosheet obtained by ultrasonic treatment of the Ce_2O_2S@carbon sample in ethanol. Many pores can be observed on the nanosheet as shown in Fig. 2c, which is in agreement with the SEM results. Enlarged view of the edge area of the nanosheet (Fig. 2d) demonstrated that the Ce_2O_2S nanosheet was well wrapped by a thin layer of carbon. The SAED pattern (Fig. 2e) indicates the well-crystallized single crystalline nature of an isolated nanosheet. The electron diffraction spots are corresponding to the (110), (011), ($10\bar{1}$) facets of Ce_2O_2S, respectively. Fig. 2f shows the HAADF STEM image and corresponding elemental mapping analysis of a randomly selected area of Ce_2O_2S@carbon. S and O detections emerge at the same position where Ce is also detected. The elemental mapping demonstrates that Ce_2O_2S is wrapped by carbon, which is in good agreement with Fig. 2d.

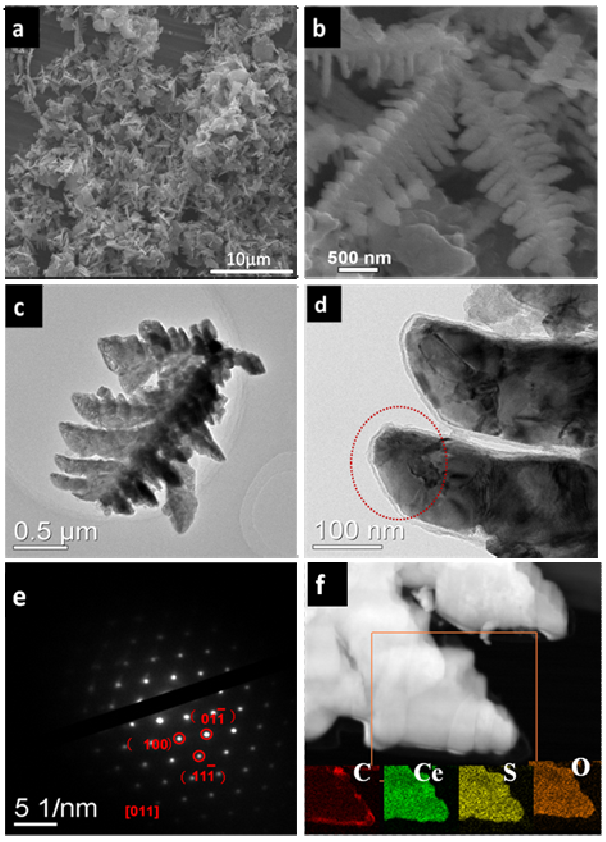

Fig.3 (a,b) SEM images of the dicranopteris-like Ce_2O_2S@carbon composites, (c,d) TEM images, (e) SAED pattern of a typical isolated Ce_2O_2S@carbon leaf (corresponding to fig.2d) and (f) STEM-HAADF image and element mapping images of Ce_2O_2S@carbon.

Fig. 3 shows the morphology of samples obtained by using deionized water and triethylamine. Fig. 3a demonstrates that the product is composed of uniform dicranopteris-like structures. The 'leaves' with various lengths (from 100 to 600 nm) and widths are connected along the main branch. Fig. 3b clearly demonstrates the morphology of a single dicranopteris-like Ce_2O_2S@carbon, which reveals that the well-defined dendritic structure grows with a long main trunk and ordered 'leaves'. The short 'leaves' distributed on both sides of the trunk. From the magnified TEM image (Fig. 3d) of the 'leaves', the Ce_2O_2S 'leaves' with width of 120 nm were uniformly wrapped by a thin layer carbon with an thickness of about 4 nm. Additionally, the SAED pattern (inset in Fig. 3e) of one of the "leaves" shows that the Ce_2O_2S 'leaves' are single crystals. The elemental mapping images in Fig. 3f also suggested that the carbon wrapped Ce_2O_2S was successfully achieved.

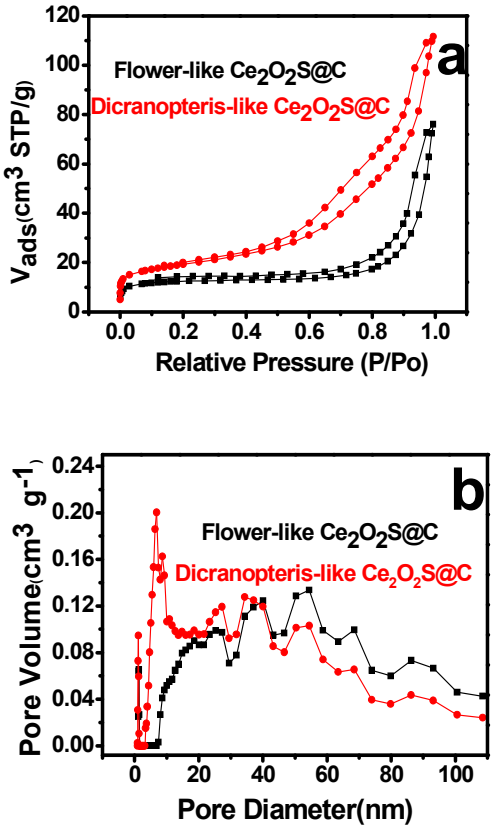

Fig.4 (a) Nitrogen adsorption/desorption isotherms and (b) DFT pore-size distribution curves of flower-like and dicranopteris-like Ce_2O_2S@carbon composites.

The surface area of flower-like and dicranopteris-like Ce_2O_2S@carbon composites was measured using the Brunauer–Emmett–Teller (BET) method. Fig. 4a shows the N_2 adsorption–desorption isotherm at 77 K. The isotherm of flower-like Ce_2O_2S@carbon composites can be classified as a typical II isotherm with a hysteresis loop, which suggests the presence of a mesoporous structure. While, the dicranopteris-like Ce_2O_2S@carbon composites exhibits mainly microporous and relatively less mecro- and macro- porous structure. The BET specific surface areas of flower-like and dicranopteris-like Ce_2O_2S@carbon composites were 39.6 m^2 g^{-1} and 66.3 m^2 g^{-1}, respectively. The pore size distribution curves (Fig. 4b), determined using the DFT method, show more detailed information about the pore structure of the flower-like and dicranopteris-like Ce_2O_2S@carbon composites. The investigated flower-like Ce_2O_2S@carbon have the mesopore peaks and macropore peaks in the range of 20-80 nm. However, the dicranopteris-like samples show a pore size distribution with a dominant micropore feature and relatively less prominent macropore features.

To investigate the electrochemical performance of the flower-like and dicranopteris-like Ce_2O_2S@carbon, a series of electrochemical characterizations were carried out based on a coin-type cell with a lithium foil as the counter electrode. In the cyclic voltammetry (Fig. 5a) of the flower-like Ce_2O_2S@carbon/Li cell between 0.01 and 3.0 V, two very tiny reduction/oxidation peak pairs are observed at 1.6/2.2 V and 0.75/1.15 V for the lithium insertion/extraction in the Ce_2O_2S nanosheets. It showed a graphite-like behavior. This is also confirmed by the charge/discharge curves as shown in Fig. 5b that hardly find the plateau on the charge/discharge curves, indicating a single-voltage output behavior.

Fig. 5b presents charge and discharge curves of the flower-like Ce_2O_2S@carbon electrode at current densities of 100 mA/g, 200 mA/g, 500 mA/g, 1000 mA/g, 2000 mA/g, 4000 mA/g and 8000 mA/g. The flower-like Ce_2O_2S@carbon exhibited remarkable rate capacity especially at high rates. It showed a discharge capacity of 240 mAh/g at a rate of 1000 mA/g. Moreover, the Ce_2O_2S@carbon electrode showed no obvious platform on the charge and discharge curves, which are in accordance with the CV results.

Fig. 5c shows the cycling stability of the flower-like and dicranopteris-like Ce_2O_2S@carbon tested at a current density of 50 mA/g between 0.01 and 3.0 V. The flower-like Ce_2O_2S@carbon delivers its highest discharge capacity of 1029 mAh/g in the first cycle, but, the discharge capacity was reduced to less than 600 mAh/g. The irreversible capacity loss is a common phenomenon, which can be ascribed to the formation of solid electrolyte interphase (SEI) on the surface of active materials and irreversible lithium insertion into the nanocomposite [19, 20]. From the second cycle, the capacity for both the flower-like and dicranopteris-like Ce_2O_2S@carbon electrodes increased rather than decreased. For example, the flower-like Ce_2O_2S@carbon electrode reached its capacity up to 627 mAh/g after 180 cycles. Whereas, the reported bare CeO_2 nanoparticles just deliver a discharge capacity of 370 mAh/g after 100 cycles[10]. The capacity for flower-like and dicranopteris-like Ce_2O_2S@carbon electrodes are still increasing after 180 cycles, the further testing is still in progress. The dicranopteris-like Ce_2O_2S@carbon and flower-like Ce_2O_2S@carbon with porous structure on the nanosheets can increase the active sites, electrode–electrolyte contact area and fast transport of lithium ions, leading to superior reversible capacity and stability.

The electrochemical impedance spectroscopy (EIS) measurements were carried out for the flower-like and dicranopteris-like Ce_2O_2S@carbon electrodes at open circuit voltage before discharging. The Nyquist plots obtained from EIS of the flower-like and dicranopteris-like Ce_2O_2S@carbon electrodes are shown in Fig. 5d. According to the semicircle which is attributed to the summation of the contact, the solid-electrolyte interphase resistance, and the charge-transfer resistance. It is apparent that both of the flower-like and dicranopteris-like Ce_2O_2S@carbon electrodes have a low resistance. The carbon layer coating outside of Ce_2O_2S can promote fast charge-transfer. And the porous structure can contribute to mass transfer for lithium ion insertion and extraction.

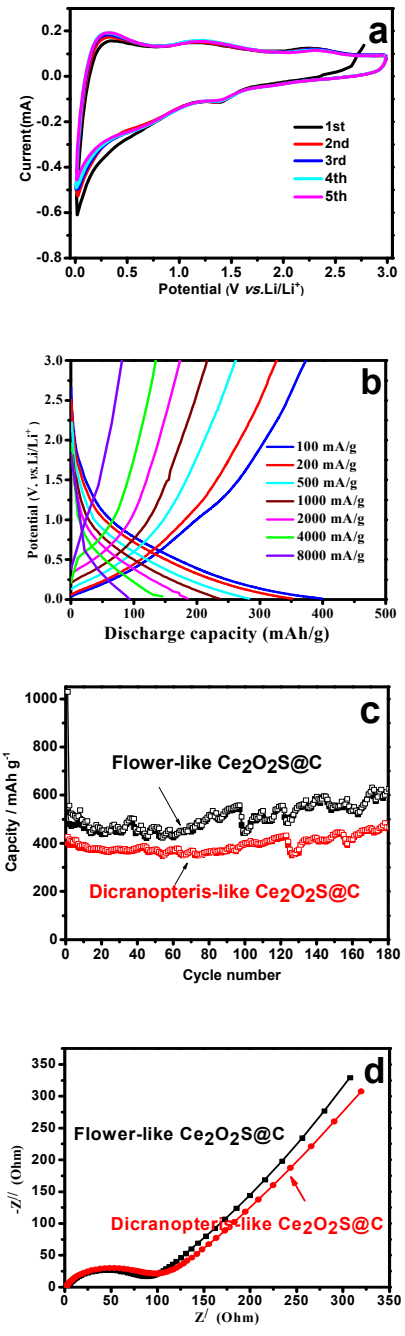

Fig. 5 (a) Cyclic voltammograms of the flower-like Ce_2O_2S@carbon composites electrode between 0.01 and 3 V at a scan rate of 0.1 mV/s for the 1st to 5th cycles, (b) rate performance of the flower-like Ce_2O_2S@carbon electrode electrode at various rates, (c) cycling performance of the flower-like and dicranopteris-like Ce_2O_2S@carbon electrodes at a rate of 50 mA/g between 0.01 and 3.0 V and (d) Nyquist plots for the flower-like and dicranopteris-like Ce_2O_2S@carbon electrodes obtained in the frequency range from 0.1 Hz to 100 kHz before discharging.

4. Conclusions

The flower-like and dicranopteris-like Ce_2O_2S uniformly anchored on graphitized carbon have been successfully synthesized for the first time and their electrochemical performance in lithium-ion batteries was preliminarily studied. The flower-like and dicranopteris-like Ce_2O_2S@carbon exhibited excellent cycling stability, rate performance and high reversible capacity. They deliver stable discharge capacities up to 627 mAh/g after 180 cycles which is much larger than that of commercially used mesocarbon microbeads. As preliminary results on lithium-ion batteries, the Ce_2O_2S@carbon material is possible to be extended its applications in other fields.

Acknowledgements

This work was supported by the Major International (Regional) Joint Research Project (51210002), the National Basic Research Program of China (2015CB932304), the Link Project of the National Natural Science Foundation of China and Guangdong Province (U1034003) and the Specialized Research Fund for the Doctoral Program of Higher Education of China (20110171110024).

Note and References

a Advanced Energy Materials Research Laboratory, School of Physics and Engineering, Sun Yat-sen University, Guangzhou 510275, China. Tel: +86-20-84036736; Fax: +86-20-84113369; E-mail: stsspk@mail.sysu.edu.cn (P.K.S.)
b Key Laboratory of Quantum Engineering and Micro-Nano Energy Technology, School of Materials, Optoelectronics and Physics, Xiangtan University, Xiangtan 411105, China.
[1] The authors contributed equally.

1 M. Hu, X. Pang, Z. Zhou, Journal of Power Sources, 2013, 237 229.
2 X. Huang, J. Chen, H. Yu, R. Cai, S. Peng, Q. Yan, H.H. Hng, J. Mater. Chem. A, 2013, 1, 6901.
3 N. Mahmood, C. Zhang, Y. Hou, Small, 2013, 9, 1321.
4 A. Dey, S. Karan, S. De, Solid State Ionics, 2008, 178, 1963.
5 D. Arumugam, G.P. Kalaignan, Electrochimica Acta, 2010,55, 8709.
6 C. Hua, X. Fang, Z. Yang, Y. Gao, Z. Wang, L. Chen, Electrochemistry Communications, 2012, 25, 66.
7 C. Li, N. Sun, J. Ni, J. Wang, H. Chu, H. Zhou, M. Li, Y. Li, Journal of Solid State Chemistry, 2008, 181, 2620.
8 F. Zhou, X. Zhao, H. Xu, C. Yuan, The Journal of Physical Chemistry C, 2007, 111, 1651.
9 M. Sasidharan, N. Gunawardhana, M. Yoshio, K. Nakashima, Chemistry Letters, 2012,41, 386.
10 G. Wang, J. Bai, Y. Wang, Z. Ren, J. Bai, Scripta Materialia, 2011, 65, 339.
11 Y.-K. Sun, Y.-S. Jeon, Electrochemistry Communications, 1999, 1, 597.
12 K. Abraham, D. Pasquariello, Chemistry of Materials, 1993, 5, 1233.

13 K. Ogisu, A. Ishikawa, Y. Shimodaira, T. Takata, H. Kobayashi, K. Domen, The Journal of Physical Chemistry C, 2008, 111, 11978.
14 S.K. Singh, A. Kumar, B. Gahtori, G. Sharma, S. Patnaik, V.P. Awana, Journal of the American Chemical Society, 2012, 134, 16504.
15 Cheng J, Li Y, Huang X, et al., Jouranal of Materials Chemisty A, 2015, 3, 1492.
16 H.-C. Liu, S.-K. Yen, Journal of Power Sources, 2007, 166, 4784.
17 L. Tian, H. Zou, J. Fu, X. Yang, Y. Wang, H. Guo, X. Fu, C. Liang, M. Wu, P.K. Shen, Advanced Functional Materials, 2010, 20, 617.
18 J.-O. Lee, J.-U. Seo, J.H. Song, C.-M. Park, C.K. Lee, Electrochemistry Communications, 2013, 28, 71.
19 J. Zhu, Y. Li, S. Kang, X.-L. Wei, P.K. Shen, Journal of Materials Chemistry A, 2014, 2, 3142.
20 X. Li, D. Geng, Y. Zhang, X. Meng, R. Li, X. Sun, Electrochemistry Communications, 2011, 13, 822.